Antimony-doped tin dioxide ceramics used as standalone membrane electrodes in electrofiltration reactors enhance the oxidation of organic micropollutants

M.C. Martí-Calatayud [a], E. Dionís [a], S. Mestre [b], V. Pérez-Herranz [a,*]

[a] Grupo IEC, Instituto Universitario de Seguridad Industrial, Radiofísica y Medioambiental, Universitat Politècnica de València, Camino de Vera S/N, 46022, València, Spain
[b] Instituto Universitario de Tecnología Cerámica, Universitat Jaume I. Campus Universitario Riu Sec, Av.Vicent Sos Baynat s/n, 12006, Castellón, Spain

ABSTRACT

In the present work, microporous ceramics made of antimony-doped tin dioxide produced using a facile synthesis procedure were evaluated during the degradation of norfloxacin in a novel electrofiltration process. The antimony-doped tin dioxide ceramics were used as standalone electrodes accomplishing a dual function: as anodes and microfiltration membranes. The simultaneous generation of hydroxyl radicals and permeation of the electrolyte through the ceramic electrodes favors the effective utilization of their high active area in the degradation of organic compounds. The progress of the electrofiltration process was compared with that of a conventional flow electrolysis reactor using the ceramic electrodes and boron-doped diamond. By changing from a conventional flow reactor to an electrofiltration configuration, the effective utilization of the generated hydroxyl radicals is evidenced by the delayed transition from electrochemical-to mass transfer-controlled degradation rates. Evaluation of intermediate and by-product concentrations confirms the formation of acetate ions as a prior stage in the mineralization pathway using both types of electrodes. After 4 h of electrolysis, norfloxacin degradation rates of 98.3% and mineralization degrees of 82% were attained using the antimony-doped tin dioxide anodes at the highest permeate flow of 60 mL min^{-1}, approaching the outstanding performance of commercial boron-doped diamond electrodes.

1. Introduction

The removal of emerging pollutants by Electrochemical Advanced Oxidation Processes (EAOP) has been the topic of a large number of studies in recent years (Brillas, 2021; Brillas and Martínez-Huitle, 2015; Sirés et al., 2014). EAOPs are based on the electrochemical generation of strong oxidizing agents, such as the hydroxyl radical (•OH), which are capable of mineralizing organic and organometallic compounds into CO_2, water, and inorganic ions. Unlike other processes that have been applied to remove organic pollutants from effluents by transferring them into another phase or stream, like adsorption, coagulation, or conventional membrane processes (Egea-Corbacho et al., 2019; Martí-Calatayud et al., 2020); EAOPs involve the use of electrons as clean reagents to achieve the chemical destruction of organic molecules.

The effectiveness of EAOPs depends on several factors, one of the most important being the nature of the anode. Among the different anode materials, thin-film BDD is considered a nonactive anode which presents the highest known potential for the OER (Garcia-Segura et al., 2015). BDD anodes produce large amounts of weakly adsorbed •OH radicals with high reactivity towards organics oxidation, which results in superior mineralization efficiencies (Panizza and Cerisola, 2005). Yet, their high cost and the difficulty to find an appropriate substrate for the deposition of thin and stable diamond layers hampers the wide utilization of BDD electrodes in large-scale applications.

Within the alternatives to BDD, SnO_2 anodes are another type of nonactive electrodes that are effective in the electrooxidation of organics present in wastewaters (Duan et al., 2014; Wang et al., 2016). However, although tin oxide is a n-type semiconductor, its large band gap (~3.5 eV) implies a high resistance to charge transfer. Doping with Sb significantly increases the conductivity of SnO_2, which can boost electron transfer for electrochemical reactions and produce a greater amount of hydroxyl radicals, thus potentially improving the overall

* Corresponding author.
  E-mail address: vperez@iqn.upv.es (V. Pérez-Herranz).

electrocatalytic characteristics (Comninellis and De Battisti, 1996).

Nevertheless, the short service life of Sb-doped SnO_2 anodes when coated onto a support also limits their broad application (Correa-Lozano et al., 1997). This inconvenience can be easily avoided by using Sb-doped SnO_2 in the form of massive ceramic electrodes, since the raw materials are cheap and their production is relatively simple (Mora-Gómez et al., 2018). Additionally, Sb-doped SnO_2 monoliths showcase high chemical stability and active areas because of their porous structure. SnO_2-based microporous ceramic electrodes have been recently applied in the removal of organic pollutants using conventional parallel flat plate electrode reactors in undivided and divided cell arrangements (Carrillo-Abad et al., 2020a; Droguett et al., 2020; Mora-Gómez et al., 2020). Unfortunately, with this electrode configuration a large part of the active area remains unproductive. To take advantage of the high active area of microporous electrodes, the electrolyte can be forced to flow through the electrode structure in a so-called electrofiltration (EF) process. In this manner, the electrode accomplishes a dual function, acting as a microfiltration membrane and as an anode simultaneously.

So far, EF has been mainly applied in pressure-driven membrane processes to enhance the separation efficiency of specific compounds and minimize membrane fouling. In the case of non-conducting membranes, a flat sheet membrane is placed as a separator between the two electrode compartments. Under the proper configuration of the electric field, undesired charged species are subjected to an additional migration force and can be either attracted to media collectors or kept away from the membrane surface. In this case, fouling is reduced by electrophoresis and electroosmosis, while the main electrochemical reaction is water electrolysis to produce oxygen at the anode and hydrogen at the cathode (Corbatón-Báguena et al., 2016; Holder et al., 2013; Khalifa et al., 2021).

In the case of electrically conducting membranes, the membrane acts as an electrode, usually as a cathode, where bubbles are generated and used as a means of physical cleaning (Oussedik et al., 2000; Tarazaga et al., 2006). Electrically conducting membranes can also be used as anodes to mitigate fouling via the inactivation of microorganisms or the degradation of organic matter (Yang et al., 2015). Vecitis et al. (2011a) and Rahaman et al. (2012) used a multiwalled carbon nanotube microfilter for the removal and inactivation of viruses and bacteria. They found that the simultaneous application of electrolysis during filtration resulted in the increased inactivation of both bacteria and viruses. Regarding the removal of organic compounds by EF, carbon nanotube filters have also been applied to remove and oxidize methyl orange and methylene blue (Liu and Vecitis, 2012; Vecitis et al., 2011b). Bakr and Rahaman (2016) applied a multiwalled carbon nanotube filter to remove ibuprofen through conventional filtration and electrochemical filtration processes. They propose the participation of indirect bulk oxidation reactions and the direct electron transfer to the organic molecules as the main pathways involved in the degradation of organics over time. Omi et al. (2017) produced conductive ultrafiltration membranes via layer-by-layer deposition of multiwalled carbon nanotubes onto polysulfone, and then demonstrated the ability of the resulting materials to simultaneously inactivate *Escherichia coli* and degrade methyl orange. The main limitation of carbonaceous materials stems from their intrinsic electrochemical instability, because they are liable to be oxidized when used as anodes (Liu et al., 2013).

TiO_2-based ceramic membranes represent an alternative to carbon-based materials in EF processes. D. Li et al. (2016) prepared tubular porous electrodes made of Ti/SnO_2–Sb and investigated their performance during the degradation of pyridine present in wastewaters. A TiO_2 based ceramic membrane coated with an antimony-doped tin oxide catalytic layer was also applied to the degradation of methyl orange as a model organic pollutant, achieving removal rates of up to 71% (X. Li et al., 2016). Xu et al. (2017) investigated the use of TiO_2-NT/SnO_2–Sb electrodes in the degradation of pyrimidine. Most of these studies have in common that, TiO_2 is used as a ceramic substrate for the coating of electrocatalytic materials. Usually, this approach involves troublesome deposition procedures, while the coating of thin and long-lasting SnO_2

layers onto a porous support still remains as a challenging issue.

In this work, Sb-doped SnO_2 microporous ceramic electrodes have been manufactured using conventional procedures of the traditional ceramic industry and have been applied to the removal of norfloxacin (NOR) through an electrofiltration process. Previous works have shown the effectiveness of SnO_2 ceramic electrodes in the degradation and mineralization of NOR in conventional electrooxidation processes (Carrillo-Abad et al., 2020a, 2020b; Mora-Gómez et al., 2019). The choice of NOR as a model pollutant facilitates the comparison between different electrodes and configurations. For the first time, a standalone Sb-doped SnO_2 ceramic electrode is implemented in an EF process. The results obtained with this electrode and operation mode are compared with those obtained in a conventional EAOP without filtration using SnO_2 ceramic anodes and BDD anodes.

2. Materials and methods

The synthesis procedure of the ceramic membrane electrodes, and methods used to characterize their structure and the electrochemical performance are described in the following subsections.

2.1. Preparation of the ceramic membrane electrodes

The membrane electrodes were manufactured with SnO_2 (purity 99.85%, Quimialmel S.A., Spain) and Sb_2O_3 (purity 99%, Alfa-Aesar, Germany) as dopant, in a mole ratio 99/1. The ligand was polyvinylalcohol (PVA, Mowiol 8–88, Clariant Iberica S.A. Spain), which was added in a 0.8% in weight.

A planetary mill (Pulverisette 5, Fritsch GmbH, Germany) was used to mix the raw materials using zirconia jars and water. The mixing conditions were 230 rpm during 1 h. To reduce the potential degradation of PVA, the obtained suspension was dried in an oven at moderate temperature (80 °C) for 24 h. The dry powder was sieved through a 600 µm mesh and moistened to 4.7% (kg water/kg dry solid). Flat specimens of $100 \times 100 \times 4.5$ mm were obtained by dry pressing at 250 kg cm^{-2} in a laboratory automatic press SS-EA (Nannetti Srl, Italy). Finally, the samples were sintered in a furnace (RHF1600, Carbolite Furnaces, UK). The temperature profile consisted of heating at 5 °C min^{-1} from room temperature to 1,200 °C, keeping the samples for 1 h at the maximum temperature and cooling down subsequently.

2.2. Characterization of the ceramic membrane electrodes

Bulk density of sintered specimens was measured by mercury immersion (Archimedes' method). The electrical resistivity of sintered samples was measured by a four-point method with a HIOKI RM3545 equipment (Hioki E.E. Corporation, Japan) and a home-made setup. The registered data allowed the calculation of weight loss, relative density, and linear contraction after the thermal cycle.

The pore size distribution of the sintered samples was obtained by mercury intrusion (AutoPore IV 9500, Micromeritics, USA) and the specific surface area was determined according to the BET method (Brunauer-Emmet-Teller) using nitrogen gas as adsorbate (Tristar 3000, Micromeritics, USA) and a degassing temperature of 150 °C for 3 h. SEM images of polished sections of the sintered electrodes were taken with a FEG-SEM device (QUANTA 200F, FEI Co, USA).

2.3. Chemicals and solutions

EF experiments were carried out using NOR as a model pollutant. NOR active compound was purchased from Sigma-Aldrich and used for the standard solutions of the UV-VIS calibration curve. Na_2SO_4 of analytical grade (Panreac) was used as supporting electrolyte. All solutions were prepared using distilled water.

Working solutions were obtained from commercial NOR pills diluted in distilled water and subsequently filtered under negative pressure with

a 2.7 μm filter paper. The supporting electrolyte concentration was 0.1 M. The initial pH of the working solution was about 5.

2.4. Electrofiltration experiments

The experiments were performed in a filter press electrochemical reactor shown schematically in Fig. 1. The EF flow reactor has a plug flow configuration and is composed of two compartments separated by a flat microporous ceramic membrane electrode with a geometric surface area of 58 cm^2. This electrode has a dual function as an anode and as a microfiltration membrane. The cathode was a 10×10 cm flat squared stainless-steel electrode with the same geometric surface area of the anode. The cathode was placed in front of the anode with a separation of 0.5 cm in the so-called reaction chamber. The electrodes were connected to a DC regulated power supply. The feed solution (1 L) containing 100 mg L^{-1} NOR and the supporting electrolyte was stored in an external reservoir and recirculated through the reaction chamber by a centrifugal pump (Iwaki). A peristaltic pump (Ismatec Reglo) operating under vacuum was used to permeate part of the electrolyte through the ceramic membrane electrode from the reaction towards the filtration chamber.

During the EF experiments the centrifugal pump and the peristaltic pump worked simultaneously. The solution was pumped from the storage tank and flowed through the reaction chamber, while a part of the solution permeated through the anode by vacuum filtration. The EF experiments were compared with electrooxidation experiments using a conventional flow electrochemical reactor without filtration. To operate under such conditions, the peristaltic pump remained turned off while the centrifugal pump was in operation. In the test without filtration, the ceramic electrode behaved like a conventional flat electrode. With this configuration a Nb/BDD electrode with a boron content of 2,500 ppm (from NEOCOAT SA®, Switzerland) was also used as anode, serving as a reference for comparison purposes.

The EF experiments were performed in galvanostatic mode at an applied current density of 35 mA cm^{-2}. The recirculation flow rate through the reaction chamber (Q$_V$) was set at a constant value of 60 L h^{-1} by means of the centrifugal pump, while the filtration flow rate (Q$_F$) was ensured by the peristaltic pump and tested at three different levels: 0 (absence of filtration), 30 and 60 mL min^{-1}. The operating parameters, such as cell voltage, current and pH, were recorded during the experiment, and samples were taken from the storage tank every 30 min. All experiments were performed at room temperature for 4h. Electrochemical degradation of NOR was monitored by a Unicam UV4-200 UV–vis spectrometer and residual concentration of NOR was determined by measuring the absorbance at a wavelength of 275 nm. Additionally, NOR mineralization was followed by measuring total organic carbon (TOC) and inorganic ions (NH$_4^+$, NO$_3^-$, F$^-$ and short-chain
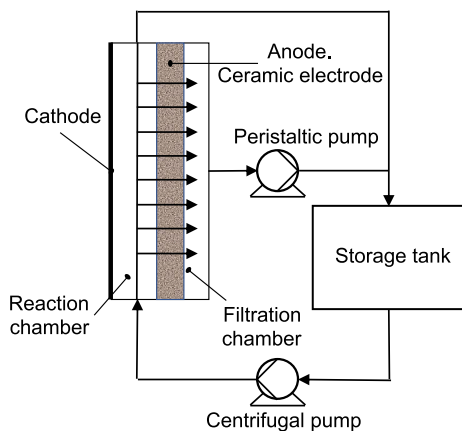
carboxylic acids) using a Shimadzu TNM-L ROHS TOC analyzer and a Metrohm Ionic Chromatograph 883 Basic IC Plus.

In order to compare the performance of EF with that of the conventional flow electrolysis, the extent of electrochemical mineralization (ϕ_{NOR}) and the mineralization current efficiency (MCE) were calculated. ϕ_{NOR} represents the fraction of NOR that is completely mineralized and was calculated as:

$$\phi_{NOR} = \frac{\%TOC_{removed}}{\%NOR_{removed}} \tag{1}$$

A value of 0 in this parameter indicates a process without combustion, while a value of 1 represents the complete mineralization of the organic micropollutant.

The MCE is the ratio between the fraction of the applied current that is effectively used in the mineralization of NOR and the total applied current. It is calculated according to equation (2):

$$MCE = \frac{n\,F\,V(TOC_0 - TOC_t)}{7.2 \times 10^{-5} m\,I\,t} \tag{2}$$

where n is the number of electrons transferred in the mineralization process, F is the Faraday constant, V is the volume of the reactor (in L), I is the applied current (A), TOC_0 and TOC_t (mg L^{-1}) are the TOC concentration at the beginning of the process and at a given time t, m is the number of carbon atoms in a NOR molecule (16) and 7.2×10^{-5} is the conversion factor for dimensional homogenization (60 s min$^{-1} \times$ 12,000 mg mol^{-1}). A value of $n = 66$ was taken, assuming the complete mineralization of NOR according to reaction (3) (Mora-Gómez et al., 2019):

$$C_{16}H_{18}FN_3O_3 + 29H_2O \rightarrow 16CO_2 + 3NH_4^+ + F^- + 64H^+ + 66e^- \tag{3}$$

3. Results and discussion

The characterization of the structure of the membrane electrodes and their electrochemical performance in the degradation of NOR under different filtration flow rates, as well as the comparison with the performance of a commercial BDD electrode are presented in the following subsections.

3.1. Characterization of the ceramic membrane electrodes

The sintered microporous ceramic membrane electrodes presented the characteristic bluish-grey color of the solid mixture (Sb,Sn)O$_2$ (Molinari et al., 2020), confirming their effective synthesis via the employed thermal treatment. Since the loss on ignition was 1.6 wt %, which is higher than the percentage of added PVA (0.8 wt %), it is estimated that the additional loss on ignition mainly corresponds to water adsorbed during the wet mixing process. However, a small fraction of antimony could also have volatilized during the sintering process.

Considering the true density of SnO$_2$ (6,850 kg m^{-3} (Lide., 2007)) and the mean bulk density of the membrane electrodes (3,727 kg m^{-3}), a porosity around 45.6% was estimated, which is in agreement with the small linear contraction value of 0.27% after firing. The pore size distribution was very narrow, with a mean pore diameter of about 0.26 μm (Fig. 2 a and Table 1). This microstructure is a result of the homogeneous and submicronic particle size of the tin oxide used as raw material, as can be seen in the SEM image of Fig. 2 b. The specific surface was 2.23 m^2 g^{-1}, what suggests a rugosity-free surface of the grains and absence of intragrain porosity, which is consistent with the SEM images.

The mean resistivity of the electrodes was 0.024 Ω cm, which was higher than values reported for bulk sintered Sb-doped tin oxide (between 4.43×10^{-3} Ω cm (Wu et al., 2013) and 2.2×10^{-4} Ω cm (Zhang et al., 2006) in samples sintered by SPS from nanopowders. Nonetheless, considering the effect of porosity on the resistivity of ceramics (Sánchez-Rivera et al., 2020), the mean resistivity is low enough to allow their use in electrofiltration processes.
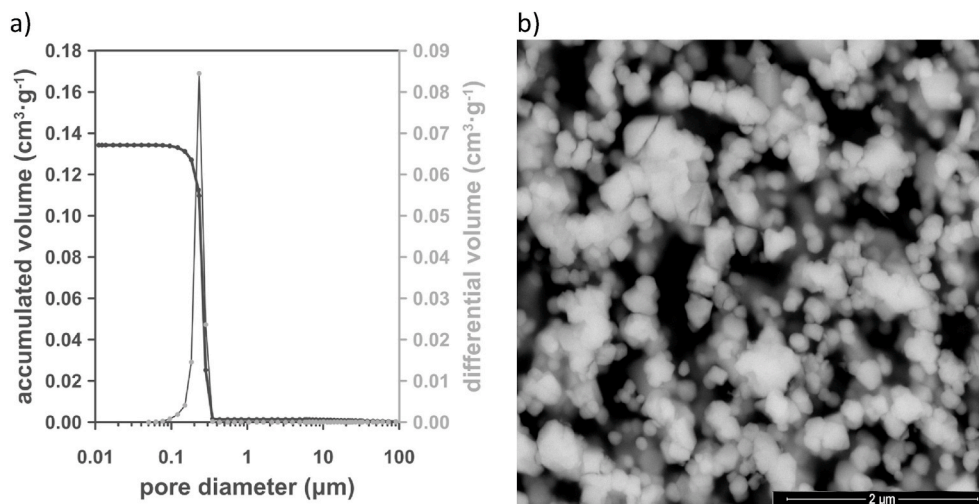

Fig. 1. Scheme of the EF flow reactor.

Fig. 2. Characterization of the structure of the ceramic membrane electrodes: a) Pore size distribution and b) SEM image of a polished section (60,000x).

Table 1
Parameters of the pore size distribution of the membrane electrode.

Total pore volume ($cm^3\ g^{-1}$)	D16 (μm)	D50 (μm)	D84 (μm)
0.134	0.29	0.26	0.23

3.2. Electrochemical oxidation of NOR

The results obtained during the EF experiments with the Sb-doped SnO_2 membrane electrodes at two different filtration flow rates and an applied current density of 35 mA cm^{-2} are compared with those obtained in a conventional flow electrolysis reactor using the same ceramic membrane electrode ($Q_F = 0$ mL min^{-1}) and a BDD electrode as anodes. The evolution of the relative concentration of NOR and TOC for the different electrode materials and reactor configurations is shown in Figs. 3 and 4. Under the same value of applied current density, the highest degradation and mineralization rates are achieved with the BDD electrode: 100% and 88%. Yet, similar NOR degradation and mineralization values are attained using the ceramic electrode at the highest filtration rate of 60 mL min^{-1}. The change in reactor configuration via permeation of the solution through the ceramic membrane electrode makes it possible to achieve a considerable improvement in both the
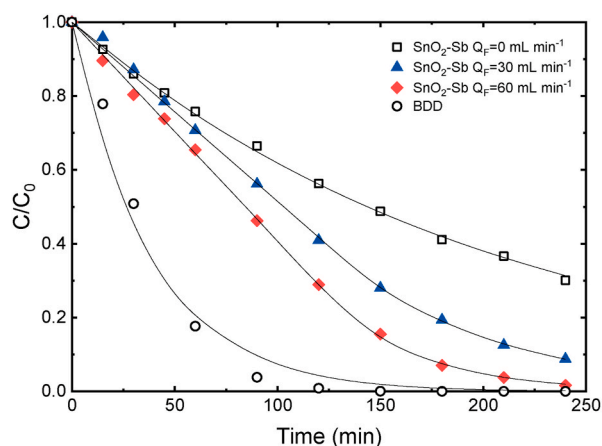

Fig. 3. Evolution of the relative concentration of NOR with time for the different electrode materials and reactor configurations. Experimental conditions constant for all experiments: i = 35 mA cm^{-2}, $Q_V = 60$ L h^{-1}. The lines represent the fitting of the experimental results to the different kinetic models discussed in section 3.3.
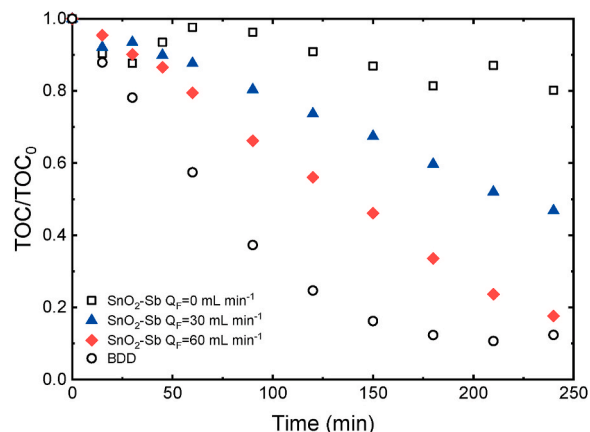

Fig. 4. Evolution of the relative TOC concentration with time for the different electrode materials and reactor configurations. Experimental conditions constant for all experiments: i = 35 mA cm^{-2}, $Q_V = 60$ L h^{-1}.

NOR degradation and mineralization rates. As can be seen, the degradation and mineralization degrees reached at the maximum filtration flow rate are close to those obtained with the BDD electrode, which is caused by the efficient utilization of all active sites in the EF experiments. The faster degradation and mineralization of NOR attained with the BDD electrode can be explained by the very weak electrode-$^{\bullet}$OH interaction, which results in a considerably higher O_2 overvoltage as compared with the ceramic electrode (Mora-Gómez et al., 2018; Ye et al., 2019).

Comparing Figs. 3 and 4, it can be inferred that for a given time, the fraction of NOR degraded is higher than the fraction of NOR mineralized for the two electrodes and for all operating conditions. The difference between the two parameters can be quantified through the extent of the electrochemical mineralization given by equation (1). Fig. 5 shows the effect of the filtration flow rate on the extent of the electrochemical mineralization. The EF results are compared with those obtained in the absence of filtration ($Q_F = 0$ mL min^{-1}) and with the BDD electrode. For all operating conditions φ_{NOR} increases with time as the intermediate organic compounds formed during the NOR degradation process are gradually converted into CO_2. In general, the best values at intermediate operating times are achieved with the BDD electrode. However, at the end of the experiments, the values obtained with the ceramic electrode at the maximum filtration flow rate of 60 mL min^{-1} approach the final value of 0.88 obtained with the BDD electrode. Within the experiments
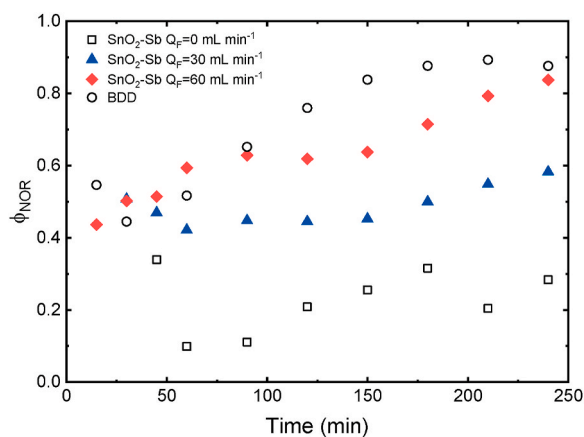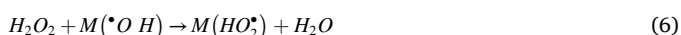
Fig. 5. Evolution of the extent of the electrochemical mineralization with time for the different electrode materials and reactor configurations. Experimental conditions constant for all experiments: i = 35 mA cm^{-2}, Q_V = 60 L h^{-1}.

conducted with the ceramic electrode, ϕ_{NOR} improves with an increase in the filtration flow rate.

The effect of the filtration flow rate on the evolution of the MCE (calculated using Eq. (2)) is shown in Fig. 6. Although the MCE is lower than 10%, these values are typical of electrochemical oxidation processes of organic compounds in low TOC content solutions (Martí-nez-Huitle et al., 2015). These results may stem from competitive electrode reactions involving the transformation of •OH radicals into O$_2$, or their dimerization and decomposition by H$_2$O$_2$ through reactions (4–6). MCE improves considerably with the filtration flow rate, increasing from an average value of 0.6% in the absence of filtration to average values of 2.5% and 5% for the filtration flow rates of 30 and 60 mL min^{-1}. With the BDD electrode, the average MCE value is 7%.

$$M\left(^{\bullet}OH\right) \rightarrow M + \frac{1}{2}O_2 + H^+ + e^- \tag{4}$$

$$2M\left(^{\bullet}OH\right) \rightarrow 2M + H_2O_2 \tag{5}$$

$$H_2O_2 + M\left(^{\bullet}OH\right) \rightarrow M\left(HO_2^{\bullet}\right) + H_2O \tag{6}$$

The evolution of MCE with time also provides valuable information regarding the effect of the reactor configuration on the course of the mineralization process. In the experiments without filtration using both the ceramic and the BDD anodes, MCE reaches the highest value at the beginning of the process and then declines with time. During the first
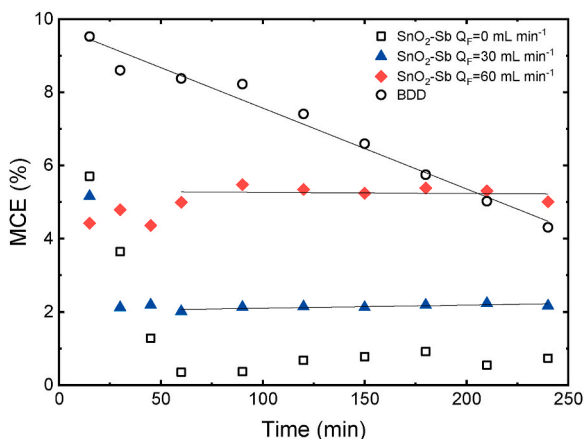

Fig. 6. Evolution of the MCE with time for the different electrode materials and reactor configurations. Experimental conditions constant for all experiments: i = 35 mA cm^{-2}, Q_V = 60 L h^{-1}.

stages, the •OH radicals generated at the electrode surface participate in the rapid conversion of intermediate products into CO$_2$. However, the decrease of MCE with time could be related to the gradual accumulation of intermediate products that are less prone to oxidation by the •OH radicals than the initial compound. The buildup of organic intermediates such as carboxylic acids near the electrode surface, or aggravated mass transfer limitations would explain the decrease of MCE with time (Hamza et al., 2009). Conversely, in EF experiments the MCE value remains almost constant with time. The forced permeation of electrolyte through the microporous electrode structure favors the supply of intermediates towards the electrode active sites, promoting a more effective use of •OH radicals in the mineralization of NOR and minimizing reactions (4–6). The values of the time-averaged mineralization current efficiency (TAMCE) are shown in Table 2. The TAMCE value increases notably with the filtration flow rate, which is in line with the hypothesis that •OH radicals have a greater chance to react with organic matter using the electrofiltration configuration.

3.3. Kinetics of NOR oxidation

The evolution of NOR concentration for the different conditions tested in this study (Fig. 3) can give some insight on the kinetics of NOR electrooxidation. When the BDD electrode is used, an exponential decrease of the NOR concentration takes place from the beginning of the experiments. This evolution obeys to a pseudo-first order kinetics, which is characteristic of mass transfer-limited processes. Conversely, with the ceramic electrode, the NOR concentration decreases linearly with time during the first stages of the electrolysis, following a pseudo-zero order kinetics. At longer times, the evolution of NOR concentration evolves into an exponential decline. From Fig. 3 it is also evident that, the time from which the decrease in NOR concentration changes from a linear to an exponential trend becomes longer with the EF experiments.

Some studies have demonstrated that the electrochemical degradation of organics follows a mixed (first and zero) order kinetics, depending on the initial compound concentration and the applied current density (Chatzisymeon et al., 2009; Lin et al., 2013). More specifically, the production of •OH substantially depends on the applied potential, because this reaction is under the control of thermodynamic feasibility, being the overvoltage for the oxygen evolution reaction (η_{OER}) the critical parameter for the current efficiency of •OH production. In a system controlled galvanostatically, if the value of η_{OER} is extremely small, the current efficiency of O$_2$ evolution could be regarded as 100% without any •OH production, as in active electrodes. On the contrary the generation of oxygen on a high η_{OER} anode is low, thus the current efficiency for •OH production would be high, as in nonactive anodes (Liu et al., 2021). The reaction rate of •OH in terms of the applied current density can be written as:

$$r\left(^{\bullet}OH\right) = \frac{d\left[^{\bullet}OH\right]}{dt} = \frac{i\,a_e\,\varphi}{n\,F} = k_{zero} \tag{7}$$

Table 2
Kinetic parameters estimated from the fittings of the NOR degradation rate curves obtained with the different electrodes and reactor configurations.

	k_{zero} (mol m^{-3} s^{-1})	k_{first} (s^{-1})	t_c (min)	TAMCE (%)
Ceramic SnO$_2$–Sb Q_F = 0 mL min^{-1}	2.29×10^{-5}	8.08×10^{-5}	20.68	0.97
Ceramic SnO$_2$–Sb Q_F = 30 mL min^{-1}	2.54×10^{-5}	2.17×10^{-4}	138.89	2.11
Ceramic SnO$_2$–Sb Q_F = 60 mL min^{-1}	3.09×10^{-5}	3.75×10^{-4}	124.28	4.83
BDD		4.50×10^{-4}		6.54

where $r(^\bullet OH)$ is the rate of $^\bullet$OH production at the electrode surface (mol $m^{-3} \, s^{-1}$), i is the applied current density (A m^{-2}), a_e is the specific surface area of the electrode (m^{-1}), φ is the current efficiency with respect to the generation of $^\bullet$OH radicals and n is the number of electrons transferred (1) according to the following reaction:

$$M + H_2O \rightarrow M\left(^\bullet O\,H\right) + H^+ + e^- \tag{8}$$

where M refers to the electrode surface. In equation (7) it is assumed that φ remains constant for a given applied current density since a supporting electrolyte is used and its concentration hardly changes during electrolysis, and there are no pH variations either. Consequently, it can be assumed that for a given applied current density the concentration of $^\bullet$OH remains approximately constant (Guinea et al., 2010; Özcan et al., 2016).

In the absence of filtration, a_e refers to the ratio between the geometric area of the electrode and the volume of the reaction chamber, and it has the same value for the ceramic electrode and for the BDD (134 m^{-1}). Consequently, in the conventional electrolysis flow reactor, e.g. without filtration, the difference between the ceramic and the BDD electrode regarding the generated amount of $^\bullet$OH radicals arises from the high φ value of the BDD. On the contrary, during the EF experiments, a_e is the specific surface area of the microporous ceramic electrode (8.31 $\times 10^6 \, m^{-1}$). Therefore, when the ceramic electrode is simultaneously used as a membrane, it is expected that a greater percentage of $^\bullet$OH radicals will be used in the oxidation of NOR instead of participating in the termination reactions (4–6) because of the improved supply of organics to the vicinity of the electrode surface.

After the generation of $^\bullet$OH radicals, it can be assumed that the main reaction responsible for the degradation of NOR in the electrochemical cell takes place between NOR and the $^\bullet$OH radicals. The rate equation can be expressed as follows:

$$r(NOR) = \frac{d[NOR]}{dt} = -k\left[^\bullet O\,H\right][NOR] \tag{9}$$

where $r(NOR)$ is the rate of NOR degradation (mol $m^{-3} \, s^{-1}$) and k is the overall reaction rate constant ($m^3 \, mol^{-1} \, s^{-1}$). As commended above, considering that for a given applied current density the concentration of $^\bullet$OH radicals is constant, equation (9) can be rewritten as a pseudo first-order reaction:

$$\frac{d[NOR]}{dt} = -k_{first}[NOR] \tag{10}$$

where k_{first} is the pseudo first-order rate constant (s^{-1}).

As can be seen in Fig. 3, equation (10) fits well the experimental data obtained with the BDD electrode. In this case, the amount of $^\bullet$OH radicals generated is very high and the overall reaction is limited by the transport of NOR from the bulk solution to the proximities of the electrode, where it reacts with $^\bullet$OH radicals. On the contrary, in the case of the ceramic electrode, at the beginning of the electrolysis, the rate of $^\bullet$OH radicals generation is slower than the mass transfer rate of NOR molecules towards the electrode. In this stage, the overall reaction rate is limited by the generation of $^\bullet$OH radicals, and the NOR degradation follows a pseudo zero-order kinetic (see equation (11)). For long operating times, after the NOR concentration has decreased sufficiently, the overall process turns to be mass transfer-controlled and behaves according to a pseudo-first order kinetics (equation (10)). The time at which the process evolves from being controlled by the $^\bullet$OH radicals rate generation to being controlled by the NOR mass transfer, is called critical time, t_c.

$$\frac{d[NOR]}{dt} = -\frac{d\left[^\bullet OH\right]}{dt} = -k_{zero} \tag{11}$$

In summary, the evolution of NOR concentration shown in Fig. 3 fits well to equations (10) and (11), depending on the electrode material,

filtration conditions and electrolysis time. For the BDD electrode, the amount of $^\bullet$OH radicals generated is very high, and the overall reaction is always limited by the transport of NOR towards the electrode. In the case of the ceramic electrode, the amount of $^\bullet$OH radicals generated is low compared to the BDD electrode. For short operating times, the concentration of NOR is high and the amount of hydroxyl radicals generated is still insufficient for attacking the large number of NOR molecules present in the solution, so that a pseudo zero-order kinetics is observed. After a certain operating time when the NOR concentration decreases (t_c), the ratio of hydroxyl radicals to NOR increases and ensures the effective oxidation of NOR molecules. At these stages, mass transfer limitations become apparent, and the kinetic regime corresponds to a pseudo first-order reaction. The estimated values of k_{zero}, k_{first} and t_c are summarized in Table 2.

In the electrolysis experiments carried out using the ceramic electrode, the filtration of the electrolyte through the 3D anode structure entails a significant improvement of both the NOR degradation and mineralization. The faster degradation kinetics observed with the EF process can be related to two synergic phenomena: the enhanced utilization of $^\bullet$OH radicals throughout the entire active surface area; and the improved NOR mass transport induced by the forced convection of the electrolyte through the microporous electrode structure. Moreover, during the EF experiments, the residence time of NOR molecules within the electrode structure is higher (0.2–0.4 min at permeate flows between 60 mL min^{-1} and 30 mL min^{-1}) than that of NOR inside the reaction chamber in the absence of filtration (0.044 min). This makes NOR more likely to react with $^\bullet$OH radicals, either to give CO_2 directly, or to form intermediate compounds that are subsequently oxidized to CO_2, as shown in the scheme of Fig. 7. After the loss of the primary structure of NOR molecules, the subsequent mineralization of intermediates would also be favored by the tortuous microstructure of the ceramic electrode. As reported in Table 2, the values of k_{zero} and k_{first} increase with the filtration flow rate, confirming the above-mentioned synergic effect. With respect to t_c, the values obtained in the EF experiments are considerably higher than those obtained without filtration. The improved transport of NOR towards the electrode with the EF reactor delays the transition to a mass transfer-limited process.

3.4. Generation of ionic by-products

The evolution of ionic intermediates and mineralization by-products generated during the electrochemical oxidation of NOR was also followed. The degradation of NOR can involve the formation of short-chain organic acids, as well as the release of inorganic species, such as fluoride and nitrogen-containing ions.

The formation of organic acids has been reported during the removal of NOR using different electrode materials, including Sb-doped SnO_2 ceramic anodes in electrolysis and BDD electrodes in electro-Fenton processes (Carrillo-Abad et al., 2020b; Özcan et al., 2016). The release of organic acids was also observed during the treatment of other fluoroquinolones, such as enoxacin by electro-Fenton (Annabi et al., 2016), and enrofloxacin via the electrogeneration of hydrogen peroxide (Guinea et al., 2010). In this work, although several short-chain organic acids were searched in the ion chromatograms, acetate was the major organic ion detected. The evolution of the acetate concentration during the experiments is shown in Fig. 8 for the two electrodes and reactor configurations. In the conventional electrolysis reactor using the ceramic electrode, the acetate concentration increased continuously over time, without reaching a saturation value. Conversely, in the other experiments, the concentration of acetate reached a saturation value, and after that, the concentration decreased with time. The maximum concentration of acetic acid attained almost the same value in the experiments with BDD and with EF, the main difference being the time at which this saturation value is reached. The maximum was registered very fast (at about 30 min) with the BDD electrode, followed by a rapid decrease over time. During the EF experiments, the increase and
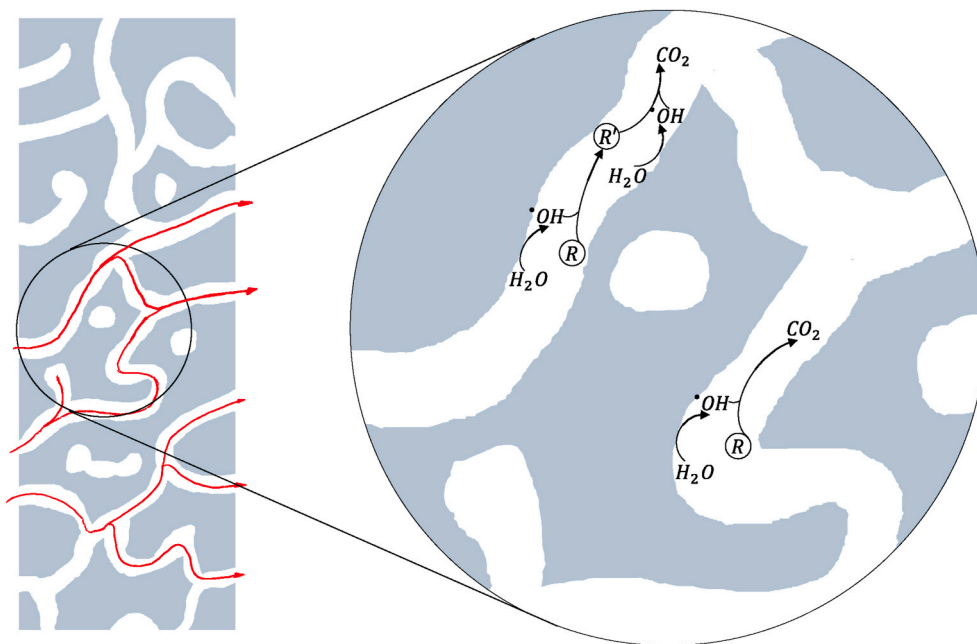
Fig. 7. Simplified reaction scheme within the microporous structure of the ceramic electrode.
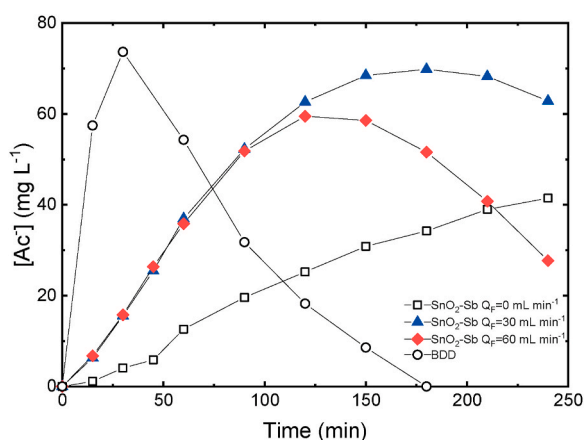

Fig. 8. Evolution of acetate concentration over time for different electrode materials and reactor configurations.

subsequent decline in the acetate concentration occurs more gradually. The sequence of remaining acetate concentration at the end of the experiments shows a good agreement with that of the mineralization rates. The TOC values calculated from the concentration of acetate ions at the end of each experiment are compared with the measured TOC values in Table 3. With the BDD anode and with the EF configuration, almost all NOR that has not been mineralized has been transformed into short-chain organic acids. However, when the ceramic electrode is used

without filtration, the concentration of other type of remaining intermediates is more significant. This observation is in line with the hypothesis depicted by the scheme of Fig. 7, indicating that the tortuous path within the microporous structure of the Sb-doped SnO_2 anodes promotes a better utilization of the generated hydroxyl radicals in the complete mineralization of organic by-products.

With respect to the nitrogen-containing ions, only NO_3^- and NH_4^+ ions were detected. Fig. 9 shows the evolution of the fractions of NH_4^+ and NO_3^- ions related to the total N-containing ions, as well as the fraction of N released compared to the N initially present in the NOR molecules (N-NOR_0) for the conventional electrolysis conducted with the BDD and the ceramic membrane electrodes. The fraction of N released was higher with the BDD electrode (Fig. 9 a). When the membrane electrode was used (Fig. 9 b), the fraction of N-containing ions increased with time, but the maximum value reached at the end of the electrolysis was 25%. With the two electrodes, the highest fraction of NH_4^+ ions was obtained at the beginning of the experiments and then decreased with time, while the fraction of NO_3^- increased continuously with time. Using the BDD electrode, the fraction of NO_3^- was higher than that of NH_4^+, whereas with the ceramic electrode, the two ions reached similar concentrations. This difference may be explained by the higher oxidizing strength yield of the BDD electrode. During the EF experiments, the distribution of N-containing ions is similar to that observed with the conventional electrolysis using the ceramic anode, though the total N released increased because of the higher mineralization rates achieved.

4. Conclusions

In this investigation, microporous ceramics made of Sb-doped SnO_2 have been used as standalone membrane electrodes in electrochemical reactors to oxidize NOR as a model organic micropollutant. The membrane electrodes were produced using standard manufacturing techniques of the traditional ceramic industry, without the need of coating additional electro-active layers on top of the porous matrix. The main conclusions drawn from the present work are summarized as follows:

- Electrofiltration favors the effective usage of the high active surface area of microporous ceramic membrane electrodes. The reaction between organic micropollutants and $^\bullet OH$ radicals is promoted by forcing the electrolyte to flow through the membrane structure. As a

Table 3
Comparison between the values of TOC calculated from the remaining acetate concentration and that experimentally measured in the samples.

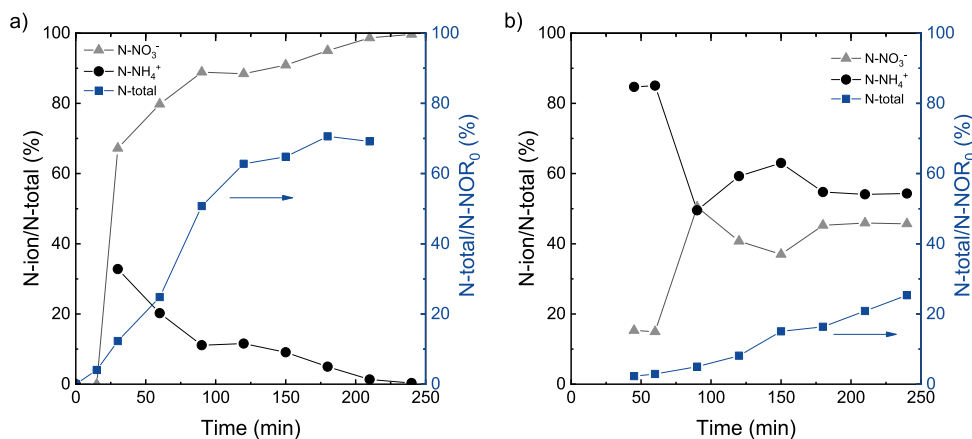|	TOC calculated (mg L^{-1})	TOC measured (mg L^{-1})
Ceramic SnO_2–Sb $Q_F = 0$ mL min^{-1}	16.96	38.55
Ceramic SnO_2–Sb $Q_F = 30$ mL min^{-1}	25.56	24.84
Ceramic SnO_2–Sb $Q_F = 60$ mL min^{-1}	10.98	13.92
BDD	3.48	7.93

Fig. 9. Evolution of the fraction of nitrogen ionic species with time (left axis), and evolution of the ratio between N released in the form of ions and N initially present in the NOR molecules (right axis): a) BDD electrode and (b) flow reactor with the ceramic membrane electrode.

result, NOR degradation and mineralization rates improve, as compared with the conventional flow reactor with the same ceramic electrode.

- The residence time of NOR molecules increases when they are filtered through the membrane, enhancing their oxidation. During the electrofiltration, the degradation rate evolves from a kinetic-controlled into a mass transfer-controlled process, as showcased by a change from a linear to an exponential decline of the NOR concentration. Increasing permeate flows delays this transition from a zero-to a first-order kinetics.
- The NOR degradation and mineralization rates obtained with the electrofiltration reactor operated at the highest permeate flow of 60 mL min^{-1} are very close to those obtained with commercial BDD electrodes. Moreover, the values of different electrochemical indicators measured with both electrodes, such as the ϕ_{NOR} and MCE are comparable.

The use of microporous ceramic Sb-doped SnO_2 membrane electrodes in an electrofiltration reactor is a promising strategy to perform the degradation of organic micropollutants present in wastewaters. Most importantly, there is still room for improvement of this novel process by tailoring the electrode properties and optimizing parameters of the filtration process.

CRediT authorship contribution statement

M.C. Martí-Calatayud: Conceptualization, Validation, Investigation, Formal analysis, Writing – review & editing. **E. Dionís:** Methodology, Investigation. **S. Mestre:** Conceptualization, Investigation, Writing – review & editing, Supervision. **V. Pérez-Herranz:** Conceptualization, Resources, Writing – review & editing, Supervision, Project administration, Funding acquisition.

Declaration of competing interest

The authors declare that they have no known competing financial interests or personal relationships that could have appeared to influence the work reported in this paper.

References

Annabi, C., Fourcade, F., Soutrel, I., Geneste, F., Floner, D., Bellakhal, N., Amrane, A., 2016. Degradation of enoxacin antibiotic by the electro-Fenton process: optimization, biodegradability improvement and degradation mechanism. J. Environ. Manag. 165, 96–105. https://doi.org/10.1016/J.JENVMAN.2015.09.018.

Bakr, A.R., Rahaman, M.S., 2016. Electrochemical efficacy of a carboxylated multiwalled carbon nanotube filter for the removal of ibuprofen from aqueous solutions under acidic conditions. Chemosphere 153, 508–520. https://doi.org/10.1016/J.CHEMOSPHERE.2016.03.078.

Brillas, E., 2021. Recent development of electrochemical advanced oxidation of herbicides. A review on its application to wastewater treatment and soil remediation. J. Clean. Prod. 290, 125841 https://doi.org/10.1016/J.JCLEPRO.2021.125841.

Brillas, E., Martínez-Huitle, C.A., 2015. Decontamination of wastewaters containing synthetic organic dyes by electrochemical methods. An updated review. Appl. Catal. B Environ. 166–167, 603–643. https://doi.org/10.1016/j.apcatb.2014.11.016.

Carrillo-Abad, J., Mora-Gómez, J., García-Gabaldón, M., Mestre, S., Pérez-Herranz, V., 2020a. Comparison between an electrochemical reactor with and without membrane for the nor oxidation using novel ceramic electrodes. J. Environ. Manag. 268 https://doi.org/10.1016/j.jenvman.2020.110710.

Carrillo-Abad, J., Mora-Gómez, J., García-Gabaldón, M., Ortega, E., Mestre, S., Pérez-Herranz, V., 2020b. Effect of the CuO addition on a Sb-doped SnO_2 ceramic electrode applied to the removal of Norfloxacin in chloride media by electro-oxidation. Chemosphere 249. https://doi.org/10.1016/j.chemosphere.2020.126178.

Chatzisymeon, E., Dimou, A., Mantzavinos, D., Katsaounis, A., 2009. Electrochemical oxidation of model compounds and olive mill wastewater over DSA electrodes : 1. The case of Ti/IrO₂ anode. J. Hazard Mater. 167, 268–274. https://doi.org/10.1016/j.jhazmat.2008.12.117.

Comninellis, C., De Battisti, A., 1996. Electrocatalysis in anodic oxidation of organics with simultaneous oxygen evolution. J. Chim. Phys. Phys. Chim. Biol. 93, 673–679. https://doi.org/10.2307/302397.

Corbatón-Báguena, M.J., Álvarez-Blanco, S., Vincent-Vela, M.C., Ortega-Navarro, E., Pérez-Herranz, V., 2016. Application of electric fields to clean ultrafiltration membranes fouled with whey model solutions. Separ. Purif. Technol. 159, 92–99.

Correa-Lozano, B., Comninellis, C., De Battisti, A., 1997. Service life of Ti/SnO₂–Sb₂O₅ anodes. J. Appl. Electrochem. 27, 970–974. https://doi.org/10.1023/A:1018410005000.

Droguett, T., Mora-Gómez, J., García-Gabaldón, M., Ortega, E., Mestre, S., Cifuentes, G., Pérez-Herranz, V., 2020. Electrochemical Degradation of Reactive Black 5 using two-different reactor configuration. Sci. Rep. 10, 1–11. https://doi.org/10.1038/s41598-020-61501-5.

Duan, T., Wen, Q., Chen, Y., Zhou, Y., Duan, Y., 2014. Enhancing electrocatalytic performance of Sb-doped SnO_2 electrode by compositing nitrogen-doped graphene nanosheets. J. Hazard Mater. 280, 304–314. https://doi.org/10.1016/J.JHAZMAT.2014.08.018.

Egea-Corbacho, A., Gutiérrez Ruiz, S., Quiroga Alonso, J.M., 2019. Removal of emerging contaminants from wastewater using nanofiltration for its subsequent reuse: full–scale pilot plant. J. Clean. Prod. 214, 514–523. https://doi.org/10.1016/J.JCLEPRO.2018.12.297.

Garcia-Segura, S., Keller, J., Brillas, E., Radjenovic, J., 2015. Removal of organic contaminants from secondary effluent by anodic oxidation with a boron-doped diamond anode as tertiary treatment. J. Hazard Mater. 283, 551–557. https://doi.org/10.1016/J.JHAZMAT.2014.10.003.

Guinea, E., Garrido, J.A., Rodríguez, R.M., Cabot, P.-L., Arias, C., Centellas, F., Brillas, E., 2010. Degradation of the fluoroquinolone enrofloxacin by electrochemical advanced oxidation processes based on hydrogen peroxide electrogeneration. Electrochim. Acta 55, 2101–2115. https://doi.org/10.1016/j.electacta.2009.11.040.

Hamza, M., Abdelhedi, R., Brillas, E., Sirés, I., 2009. Comparative electrochemical degradation of the triphenylmethane dye Methyl Violet with boron-doped diamond and Pt anodes. J. Electroanal. Chem. 627, 41–50. https://doi.org/10.1016/j.jelechem.2008.12.017.

Holder, A., Weik, J., Hinrichs, J., 2013. A study of fouling during long-term fractionation of functional peptides by means of cross-flow ultrafiltration and cross-flow electro membrane filtration. J. Membr. Sci. 446, 440–448. https://doi.org/10.1016/J.MEMSCI.2013.06.017.

Khalifa, O., Banat, F., Srinivasakannan, C., AlMarzooqi, F., Hasan, S.W., 2021. Ozonation-assisted electro-membrane hybrid reactor for oily wastewater treatment: a methodological approach and synergy effects. J. Clean. Prod. 289, 125764 https://doi.org/10.1016/J.JCLEPRO.2020.125764.

Li, D., Tang, J., Zhou, X., Li, J., Sun, X., Shen, J., Wang, L., Han, W., 2016. Electrochemical degradation of pyridine by Ti/SnO_2–Sb tubular porous electrode. Chemosphere 149, 49–56. https://doi.org/10.1016/J.CHEMOSPHERE.2016.01.078.

Li, X., Liu, G., Shi, M., Li, Jiao, Li, Juan, Guo, C., Lee, J.K., Zheng, J., 2016. Using TiO_2 mesoflower interlayer in tubular porous titanium membranes for enhanced electrocatalytic filtration. Electrochim. Acta 218, 318–324. https://doi.org/10.1016/J.ELECTACTA.2016.08.098.

Lide, D.R. (Ed.), 2007. CRC Handbook of Chemitry and Physics, 88th ed. CRC Press Inc.

Lin, H., Niu, J., Xu, J., Li, Y., Pan, Y., 2013. Electrochemical mineralization of sulfamethoxazole by Ti/SnO_2-Sb/Ce-PbO_2 anode: kinetics, reaction pathways, and energy cost evolution. Electrochim. Acta 97, 167–174.

Liu, G., Zhang, C., Zhou, Y., Yan, Q., 2021. Insight into the overpotential and thermodynamic mechanism of hydroxyl radical formation on diamond anode. Appl. Surf. Sci. 565, 150559 https://doi.org/10.1016/J.APSUSC.2021.150559.

Liu, H., Vajpayee, A., Vecitis, C.D., 2013. Bismuth-doped tin oxide-coated carbon nanotube network: improved anode stability and efficiency for flow-through organic electrooxidation. ACS Appl. Mater. Interfaces 5, 10054–10066. https://doi.org/10.1021/am402621v.

Liu, H., Vecitis, C.D., 2012. Reactive transport mechanism for organic oxidation during electrochemical filtration: mass-transfer, physical adsorption, and electron-transfer. J. Phys. Chem. C 116, 374–383. https://doi.org/10.1021/jp209390b.

Martí-Calatayud, M.C., Heßler, R., Schneider, S., Bohner, C., Yüce, S., Wessling, M., de Sena, R.F., Athayde Júnior, G.B., 2020. Transients of micropollutant removal from high-strength wastewaters in PAC-assisted MBR and MBR coupled with high-retention membranes. Separ. Purif. Technol. 246, 116863 https://doi.org/10.1016/j.seppur.2020.116863.

Martínez-Huitle, C.A., Rodrigo, M.A., Sirés, I., Scialdone, O., 2015. Single and coupled electrochemical processes and reactors for the abatement of organic water pollutants: a critical review. Chem. Rev. 115, 13362–13407. https://doi.org/10.1021/acs.chemrev.5b00361.

Molinari, C., Conte, S., Zanelli, C., Ardit, M., Cruciani, G., Dondi, M., 2020. Ceramic pigments and dyes beyond the inkjet revolution: from technological requirements to constraints in colorant design. Ceram. Int. 46, 21839–21872. https://doi.org/10.1016/j.ceramint.2020.05.302.

Mora-Gómez, J., García-Gabaldón, M., Carrillo-Abad, J., Montañés, M.T., Mestre, S., Pérez-Herranz, V., 2020. Influence of the reactor configuration and the supporting electrolyte concentration on the electrochemical oxidation of Atenolol using BDD and SnO_2 ceramic electrodes. Separ. Purif. Technol. 241 https://doi.org/10.1016/j.seppur.2020.116684.

Mora-Gómez, J., García-Gabaldón, M., Ortega, E., Sánchez-Rivera, M.-J., Mestre, S., Pérez-Herranz, V., 2018. Evaluation of new ceramic electrodes based on Sb-doped SnO_2 for the removal of emerging compounds present in wastewater. Ceram. Int. 44, 2216–2222. https://doi.org/10.1016/j.ceramint.2017.10.178.

Mora-Gómez, J., Ortega, E., Mestre, S., Pérez-Herranz, V., García-Gabaldón, M., 2019. Electrochemical degradation of norfloxacin using BDD and new Sb-doped SnO_2 ceramic anodes in an electrochemical reactor in the presence and absence of a cation-exchange membrane. Separ. Purif. Technol. 208, 68–75. https://doi.org/10.1016/J.SEPPUR.2018.05.017.

Omi, F.R., Choudhury, M.R., Anwar, N., Bakr, A.R., Rahaman, M.S., 2017. Highly conductive ultrafiltration membrane via vacuum filtration assisted layer-by-layer deposition of functionalized carbon nanotubes. Ind. Eng. Chem. Res. 56, 8474–8484. https://doi.org/10.1021/acs.iecr.7b00847.

Oussedik, S., Belhocine, D., Grib, H., Lounici, H., Piron, D.L., Mameri, N., 2000. Enhanced ultrafiltration of bovine serum albumin with pulsed electric field and fluidized activated alumina. Desalination 127, 59–68. https://doi.org/10.1016/S0011-9164(99)00192-7.

Özcan, A., Atılır Özcan, A., Demirci, Y., 2016. Evaluation of mineralization kinetics and pathway of norfloxacin removal from water by electro-Fenton treatment. Chem. Eng. J. 304, 518–526. https://doi.org/10.1016/j.cej.2016.06.105.

Panizza, M., Cerisola, G., 2005. Application of diamond electrodes to electrochemical processes. Electrochim. Acta 51, 191–199. https://doi.org/10.1016/j.electacta.2005.04.023.

Rahaman, M.S., Vecitis, C.D., Elimelech, M., 2012. Electrochemical carbon-nanotube filter performance toward virus removal and inactivation in the presence of natural organic matter. Environ. Sci. Technol. 46, 1556–1564. https://doi.org/10.1021/es203607d.

Sánchez-Rivera, M.-J., Gozalbo, A., Pérez-Herranz, V., Mestre, S., 2020. Effect of pore generator on microstructure and resistivity of Sb_2O_3 and CuO doped SnO_2 electrodes. J. Porous Mater. 27 https://doi.org/10.1007/s10934-020-00959-0.

Sirés, I., Brillas, E., Oturan, M.A., Rodrigo, M.A., Panizza, M., 2014. Electrochemical advanced oxidation processes: today and tomorrow. A review. Environ. Sci. Pollut. Res. Int. 21, 8336–8367. https://doi.org/10.1007/s11356-014-2783-1.

Tarazaga, C.C., Campderrós, M.E., Padilla, A.P., 2006. Physical cleaning by means of electric field in the ultrafiltration of a biological solution. J. Membr. Sci. 278, 219–224. https://doi.org/10.1016/J.MEMSCI.2005.11.004.

Vecitis, C.D., Schnoor, M.H., Saifur Rahaman, M., Schiffman, J.D., Elimelech, M., 2011a. Electrochemical multiwalled carbon nanotube filter for viral and bacterial removal and inactivation. Environ. Sci. Technol. 45, 3672–3679. https://doi.org/10.1021/es2000062.

Vecitis, C.D., Gao, G., Liu, H., 2011b. Electrochemical carbon nanotube filter for adsorption, desorption, and oxidation of aqueous dyes and anions. J. Phys. Chem. C 115, 3621–3629. https://doi.org/10.1021/jp111844j.

Wang, Y., Shen, C., Zhang, M., Zhang, B.T., Yu, Y.G., 2016. The electrochemical degradation of ciprofloxacin using a SnO_2-Sb/Ti anode: influencing factors, reaction pathways and energy demand. Chem. Eng. J. 296, 79–89. https://doi.org/10.1016/j.cej.2016.03.093.

Wu, J., Chen, F., Shen, Q., Schoenung, J.M., Zhang, L., 2013. Spark plasma sintering and densification mechanisms of antimony-doped tin oxide nanoceramics. J. Nanomater. 2013 https://doi.org/10.1155/2013/561895.

Xu, A., Dai, X., Wei, K., Han, W., Li, J., Sun, X., Shen, J., Wang, L., 2017. Preparation and characterization of a TiO_2-NT/SnO –Sb tubular porous electrode with long service lifetime for wastewater treatment process. RSC Adv. 7, 37806–37814. https://doi.org/10.1039/C7RA05127A.

Yang, B., Geng, P., Chen, G., 2015. One-dimensional structured IrO_2 nanorods modified membrane for electrochemical anti-fouling in filtration of oily wastewater. Separ. Purif. Technol. 156, 931–941. https://doi.org/10.1016/J.SEPPUR.2015.10.040.

Ye, Z., Steter, J.R., Centellas, F., Cabot, P.L., Brillas, E., Sirés, I., 2019. Photoelectro-Fenton as post-treatment for electrocoagulated benzophenone-3-loaded synthetic and urban wastewater. J. Clean. Prod. 208, 1393–1402. https://doi.org/10.1016/J.JCLEPRO.2018.10.181.

Zhang, J., Gao, L., Chen, M., 2006. Spark plasma sintering of high-density antimony-doped tin oxide ceramics from nanoparticles. J. Am. Ceram. Soc. 89, 3874–3876. https://doi.org/10.1111/j.1551-2916.2006.01317.x.